Electrical Engineering. His field of research is electromagnetic theory, propagation, and microwave theory. He has employed EM model studies to investigate the problem of propagation in nonuniform terrestial waveguides. He has developed transform techniques to obtain full-wave solutions to problems of depolarization, diffraction, and scattering of radio waves in nonuniform layered structures. He has employed generalized characteristic vectors and developed generalized WKB techniques to solve problems of propagation in inhomogeneous anisotropic media.

Dr. Bahar is a member of Commissions B, C, and F of the International Union of Radio Science and a member of the IEEE Antennas and Propagation Society and Microwave Theory and Techniques Society.

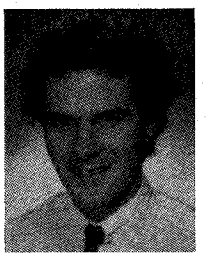

John D. Saylor (S'78–M'80) received the B.S. and M.S. degrees in 1979 and 1981, respectively, in electrical engineering from the University of Nebraska, Lincoln.

He joined Sandia National Laboratories in 1981. He is a Technical Staff Member in the Bipolar and Microwave Semiconductor Device Division (2123).

Waves Guided by Conductive Strips Above a Periodically Perforated Ground Plane

BARRY J. RUBIN, MEMBER, IEEE, AND HENRY L. BERTONI, SENIOR MEMBER, IEEE

Abstract—**This paper considers the propagation of waves along an array of conductive strips situated above a periodically perforated conductive plane. Each conductor has zero thickness and finite sheet resistance, and the dielectric is homogeneous. The surface current density on the conductors is approximated by a finite number of current elements having rooftop spatial dependence. The transverse electric field is expressed in terms of the current, and the electric field boundary condition is satisfied in an integral sense over the conductors. This generates a matrix equation whose solution gives the dispersion curve relating the propagation constant to frequency, as well as the current distribution.**

The simulation results are used to obtain equivalent transmission-line parameters applicable to printed circuit boards found in high-performance computers. A characteristic impedance is defined and it is shown that, with proper interpretation, the uniform transmission-line equations for propagation constant and characteristic impedance apply to such computer packages. The coupling between adjacent strips is calculated, and the effect of finite resistivity discussed.

I. Introduction

TRANSMISSION LINES in the form of conductive strips (signal lines) embedded in a dielectric and sandwiched between conductive planes are used in high-performance computers to carry signals between integrated-circuit chips. Often, many layers of conductor and dielectric are integrated into a compact package or printed circuit board [1], and may require interconnections between signal lines located on different layers. Arrays of holes are therefore made in the conducting planes and dielectric so that conductive elements can be inserted to electrically connect signal lines situated on different layers. The resulting transmission-line structure is, then, an array of signal lines situated between and insulated from ground planes which are perforated periodically with apertures.

One might assume that the structure can be approximated as a uniform transmission line. By calculating the appropriate capacitance, inductance, and resistance, through available means [2], [3], the propagation characteristics could then be determined. However, the validity of such an approximation must remain questionable until the structure is accurately analyzed.

In this paper, we present a numerical analysis based on rigorous electromagnetic theory for propagation along an array of signal lines situated above a single perforated ground plane in a homogeneous dielectric. We chose to consider an array of signal lines because the composite structure has two-dimensional periodicity and previous results can be applied. However, if adjacent signal lines are sufficiently separated to reduce their interaction, the resulting current distribution approaches that for an isolated signal line situated above the ground plane. Numerical results are given for the propagation constant, characteristic impedance, and the coupling between adjacent lines.

Manuscript received September 7, 1982; revised March 3, 1983. This work was submitted by Barry J. Rubin in partial fulfillment of the requirements for the Ph.D. degree in electrical engineering at the Polytechnic Institute of New York and carried out while he attended the Polytechnic under the I.B.M. Resident Study Program.

B. J. Rubin is with the General Technology Division of the I.B.M. Corporation, Hopewell Junction, NY 12533.

H. L. Bertoni is with the Department of Electrical Engineering and Computer Science of the Polytechnic Institute of New York, Brooklyn, NY 11201.

0018-9480/83/0700-0541$01.00 ©1983 IEEE

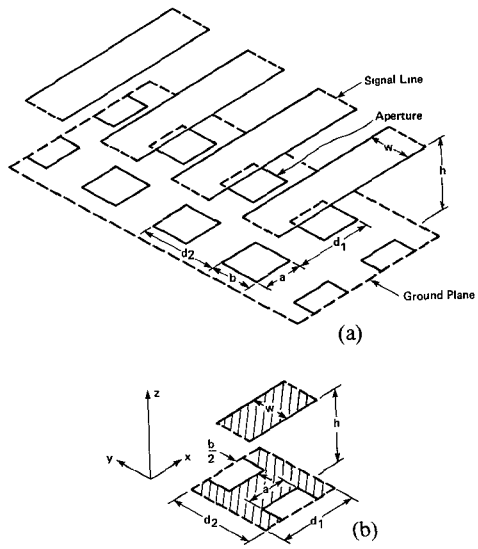

Fig. 1. Array of signal lines above a periodically perforated ground plane. (a) Isometric view. (b) Unit cell.

II. Expansion of the Signal Line and Ground-Plane Currents in Terms of Rooftop Functions

The structure considered is shown in Fig. 1(a). The ground plane, located at $z = 0$, is perforated with rectangular apertures having dimensions a and b; the signal lines, having width w, are situated a height h above. All conductors have zero thickness and finite sheet resistance R_s. The unit cell for the structure is shown in Fig. 1(b), where the periodicities in the x and y directions are d_1 and d_2, respectively.

Consistent with computer applications, the signal lines lie directly above the continuous portion of the ground plane and not over the apertures. The entire guiding structure is embedded in a homogeneous medium having free-space dielectric constant ϵ_0. In what follows, k_0, λ_0, and η_0 are the wave number, wavelength, and wave impedance in the dielectric, respectively, and the time dependency is $\exp(j\omega t)$, where ω is the angular frequency.

Since the structure has two-dimensional periodicity, the Floquet [4] condition requires the current densities on both the ground plane and signal line to be periodic functions of x and y. For propagation along the x direction, these current densities are multiplied by the same factor $\exp(-jk_x x)$, where k_x is the propagation constant. When the surface current density $\boldsymbol{J}_s$ is approximated by a finite number of current elements that are localized to rectangular regions within the unit cell, the x-directed current density J_{sx} can be expressed as a superposition of elemental currents having the form

$$I_{x\alpha} R_x(x - x_\alpha, y - y_\alpha) \exp(-jk_x x)$$

where $I_{x\alpha}$ is a complex coefficient and $R_x(x - x_\alpha, y - y_\alpha)$ is a periodic function centered at $(x_\alpha, y_\alpha, z_\alpha)$ that is nonzero only within a rectangular region or subsection of the unit cell. Furthermore, if we assume that P such elements are required to represent J_{sx}, then the y-directed current density J_{sy} can similarly be represented by Q elements having the form

$$I_{y\alpha} R_y(x - x_{P+\alpha}, y - y_{P+\alpha}) \exp(-jk_x x)$$

where $I_{y\alpha}$ and $R_y(x - x_{P+\alpha}, y - y_{P+\alpha})$ are the coefficient and subsectional functions corresponding to the αth element of J_{sy}, centered at $(x_{P+\alpha}, y_{P+\alpha}, z_{P+\alpha})$.

The functions R_x and R_y must satisfy two requirements. Firstly, the approximate current density must be consistent with the edge condition [5], which requires the current that flows along an edge in a strip of conductor to be finite, and the current that flows normally to approach zero near the edge. Secondly, the variation of the surface current must be sufficiently smooth so that its divergence does not yield any artificial (fictitious) charge. A set of functions meeting these requirements are the rooftop functions employed by Glisson and Wilton in determining the field scattered by an isolated plate [6] and by Rubin and Bertoni in determining the current distribution and reflection coefficient when a plane perforated periodically with apertures is illuminated by a plane wave [7], [8].

The rooftop functions have triangular dependency in one direction and pulse dependency in the other, and are given by

$$R_x(x, y) = q_{\tau_a}(x) p_{\tau_b}(y)$$
$$R_y(x, y) = p_{\tau_a}(x) q_{\tau_b}(y)$$

where $q_\tau(\xi)$ is the triangle function defined as

$$q_\tau(\xi) = \begin{cases} 1 - \dfrac{|\xi|}{\tau}, & -\tau \leqslant \xi \leqslant \tau \\ 0, & \text{elsewhere} \end{cases}$$

and $p_\tau(\xi)$ is the pulse function defined as

$$p_\tau(\xi) = \begin{cases} 1, & -\dfrac{\tau}{2} < \xi < \dfrac{\tau}{2} \\ 0, & \text{elsewhere.} \end{cases}$$

The parameters τ_a and τ_b define the sizes of the subsections.

Fig. 2 shows how rooftop functions can be used to represent the current that flows in the ground plane. The subsections for the x-directed current elements have dimensions $2\tau_a$ and τ_b in the x and y directions, respectively, while the subsections for the y-directed current elements have dimensions τ_a and $2\tau_b$. The centers (x_α, y_α) of the subsections used to represent J_{sx} are indicated in Fig. 2 by the dots located on lines parallel to y. The subsections used to represent J_{sy} in Fig. 2 are similarly centered at $(x_{P+\alpha}, y_{P+\alpha})$, and are indicated by the dots located on lines parallel to x. Because the currents on opposite edges of the unit cell are related via the Floquet condition, independent current coefficients $I_{x\alpha}$, $I_{y\alpha}$ are defined only at half of the points on the boundary of the unit cell. In Fig. 2, dots have been omitted from the redundant points on the boundary. For the subsections of the ground plane shown, there are $P = 30$ coefficients $I_{x\alpha}$, and an equal number Q coefficients $I_{y\alpha}$. The subsections overlap so that each patch having area $\tau_a \tau_b$ may have as many as four

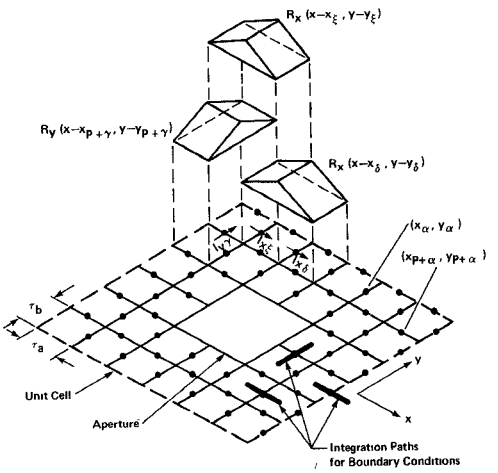

Fig. 2. Rooftop approximation for the current density on the ground plane indicating subsections of the unit cell and current elements used in the expansion of J_{sx} and J_{sy}.

rooftop functions overlaying it. Aside from the exponential factor $\exp(-jk_x x)$, J_{sx} is continuous piecewise-linear in the x direction and stepwise-constant in the y direction, while J_{sy} is continuous piecewise-linear in the y direction and stepwise-constant in the x direction. The signal line's current density can similarly be approximated through rooftop functions, so that the current density in either the signal line or the ground plane can be expressed as

$$J_s(x,y,z) \simeq \left\{ \sum_{\alpha=1}^{P} I_{x\alpha}\delta_{z,z_\alpha} R_x(x-x_\alpha, y-y_\alpha)\boldsymbol{x}_0 + \sum_{\alpha=1}^{Q} I_{y\alpha}\delta_{z,z_{P+\alpha}} R_y(x-x_{P+\alpha}, y-y_{P+\alpha})\boldsymbol{y}_0 \right\} \exp(-jk_x x) \tag{1}$$

where δ_{z,z_α} is the Kronecker delta. The current on the ground plane corresponds to those elemental currents for which $z_\alpha = 0$, while the current on the signal line corresponds to those elemental currents for which $z_\alpha = h$.

III. The Eigenvalue Problem

It has been shown [7], [8] that the transverse component of the electric field $\boldsymbol{E}_t$ produced by the current density (1) in the plane $z = 0$ can be expressed in component form as

$$E_x = -\frac{\eta_0}{2k_0}\Sigma_{n,m}\left\{ \frac{k_0^2 - k_{xn}^2}{k_{znm}} \sum_{\alpha=1}^{P} I_{x\alpha}\mathcal{R}_{xnm} \cdot \exp\left[j\left(\frac{2\pi n}{d_1}x_\alpha + \frac{2\pi m}{d_2}y_\alpha \right)\right] - \frac{k_{xn}k_{ym}}{k_{znm}} \sum_{\alpha=1}^{Q} I_{y\alpha}\mathcal{R}_{ynm} \cdot \exp\left[j\left(\frac{2\pi n}{d_1}x_{P+\alpha} + \frac{2\pi m}{d_2}y_{P+\alpha} \right)\right]\right\} \cdot \exp\left[-j(k_{xn}x + k_{ym}y + k_{znm}|z|)\right]$$

and

$$E_y = -\frac{\eta_0}{2k_0}\Sigma_{n,m}\left\{ -\frac{k_{xn}k_{ym}}{k_{znm}} \sum_{\alpha=1}^{P} I_{x\alpha}\mathcal{R}_{xnm} \cdot \exp\left[j\left(\frac{2\pi n}{d_1}x_\alpha + \frac{2\pi m}{d_2}y_\alpha \right)\right] + \frac{k_0^2 - k_{ym}^2}{k_{znm}} \sum_{\alpha=1}^{Q} I_{y\alpha}\mathcal{R}_{ynm} \cdot \exp\left[j\left(\frac{2\pi n}{d_1}x_{P+\alpha} + \frac{2\pi m}{d_2}y_{P+\alpha} \right)\right]\right\} \cdot \exp\left[-j(k_{xn}x + k_{ym}y + k_{znm}|z|)\right] \tag{2}$$

where

$$k_{xn} = k_x + \frac{2\pi n}{d_1}, \quad k_{ym} = \frac{2\pi m}{d_2}$$

$$k_{znm} = \left(k_0^2 - k_{xn}^2 - k_{ym}^2\right)^{1/2}$$

and $\mathcal{R}_{xnm}$ and $\mathcal{R}_{ynm}$ are the Fourier series coefficients of the functions $R_x(x, y)$ and $R_y(x, y)$, respectively. In order to accommodate currents located in planes other than $z = 0$, we replace the factor $|z|$ in (2) appropriately by the factors $|z - z_\alpha|$ or $|z - z_{P+\alpha}|$. With this modification, (2) becomes valid for any current distribution represented by (1). The total electric field is, then, obtained by superposition over the planes containing the current.

We now apply the electric field boundary condition

$$\boldsymbol{E}_t - \boldsymbol{J}_s R_s = 0 \tag{3}$$

to generate a finite dimension matrix equation having the $P + Q$ current coefficients $I_{x\alpha}$ and $I_{y\alpha}$ as the unknowns. As described in [7] and [8], satisfying the boundary condition at isolated points leads to numerical difficulties since it results in matrix elements which are not absolutely convergent. Instead, the x component of (3) is integrated over P line segments of length τ_a parallel to the x axis and centered at each of the points $(x_\alpha, y_\alpha, z_\alpha)$. Two such segments along x are indicated by heavy lines in Fig. 2. Similarly, the y component of (3) is integrated over Q line segments of length τ_b parallel to the y axis and centered at each of the points $(x_{P+\alpha}, y_{P+\alpha}, z_{P+\alpha})$. One such segment is indicated in Fig. 2. Mathematically, the boundary conditions take the form

$$\int_{x_\beta - \tau_a/2}^{x_\beta + \tau_a/2} (E_x - R_s J_{sx})\, dx = 0 \text{ at } z = z_\beta, y = y_\beta, \quad \beta = 1,2,\cdots,P$$

$$\int_{y_{P+\beta} - \tau_b/2}^{y_{P+\beta} + \tau_b/2} (E_y - R_s J_{sy})\, dy = 0 \text{ at } z = z_{P+\beta}, x = x_{P+\beta}, \quad \beta = 1,2,\cdots,Q. \tag{4}$$

Substituting (1) and (2) into (4), and then interchanging the orders of summation and the order of summation and

integration we obtain

$$\sum_{\alpha=1}^{P} I_{x\alpha}\left(Z_{xx\alpha\beta} - R_s F_{x\alpha\beta}\right) + \sum_{\alpha=1}^{Q} I_{y\alpha} Z_{xy\alpha\beta} = 0, \qquad \beta = 1,2,\cdots,P$$

$$\sum_{\alpha=1}^{P} I_{x\alpha} Z_{yx\alpha\beta} + \sum_{\alpha=1}^{Q} I_{y\alpha}\left(Z_{yy\alpha\beta} - R_s F_{y\alpha\beta}\right) = 0, \qquad \beta = 1,2,\cdots,Q \quad (5)$$

where

$$Z_{xx\alpha\beta} = -\frac{\eta_0}{2k_0} \sum_{n,m} Sa\left(k_{xn}\frac{\tau_a}{2}\right) \frac{k_0^2 - k_{xn}^2}{k_{znm}} \mathcal{R}_{xnm} \cdot \exp\left\{ j\left[\frac{2\pi n}{d_1}(x_\alpha - x_\beta) + \frac{2\pi m}{d_2}(y_\alpha - y_\beta) - k_{znm}|z_\alpha - z_\beta| \right]\right\}$$

$$Z_{xy\alpha\beta} = \frac{\eta_0}{2k_0} \sum_{n,m} Sa\left(k_{xn}\frac{\tau_a}{2}\right) \frac{k_{xn}k_{ym}}{k_{znm}} \mathcal{R}_{ynm} \cdot \exp\left\{ j\left[\frac{2\pi n}{d_1}(x_{P+\alpha} - x_\beta) + \frac{2\pi m}{d_2}(y_{P+\alpha} - y_\beta) - k_{znm}|z_{P+\alpha} - z_\beta| \right]\right\}$$

$$Z_{yx\alpha\beta} = \frac{\eta_0}{2k_0} \sum_{n,m} Sa\left(k_{ym}\frac{\tau_b}{2}\right) \frac{k_{xn}k_{ym}}{k_{znm}} \mathcal{R}_{xnm} \cdot \exp\left\{ j\left[\frac{2\pi n}{d_1}(x_\alpha - x_{P+\beta}) + \frac{2\pi m}{d_2}(y_\alpha - y_{P+\beta}) - k_{znm}|z_\alpha - z_{P+\beta}| \right]\right\}$$

$$Z_{yy\alpha\beta} = -\frac{\eta_0}{2k_0} \sum_{n,m} Sa\left(k_{ym}\frac{\tau_b}{2}\right) \frac{k_0^2 - k_{ym}^2}{k_{znm}} \mathcal{R}_{ynm} \cdot \exp\left\{ j\left[\frac{2\pi n}{d_1}(x_{P+\alpha} - x_{P+\beta}) + \frac{2\pi m}{d_2}(y_{P+\alpha} - y_{P+\beta}) - k_{znm}|z_{P+\alpha} - z_{P+\beta}| \right]\right\} \quad (6)$$

$$F_{x\alpha\beta} = \left\{ F_0 \delta_{x_\alpha, x_\beta} + F_1 \delta_{\tau_a + x_\alpha, x_\beta} + F_1^* \delta_{x_\alpha, \tau_a + x_\beta} \right\} \delta_{y_\alpha, y_\beta} \delta_{z_\alpha, z_\beta}$$

$$F_{y\alpha\beta} = \left\{ \frac{3}{4}\delta_{y_{P+\alpha}, y_{P+\beta}} + \frac{1}{8}\delta_{\tau_b + y_{P+\alpha}, y_{P+\beta}} + \frac{1}{8}\delta_{y_{P+\alpha}, \tau_b + y_{P+\beta}} \right\} \delta_{x_{P+\alpha}, x_{P+\beta}} \delta_{z_{P+\alpha}, z_{P+\beta}}. \quad (7)$$

In (6), $Sa(\xi) = \sin(\xi)/\xi$ is the sampling function, and in (7)

$$F_0 = \frac{1}{2} Sa\left(k_x \frac{\tau_a}{2}\right) + \frac{1}{4} Sa^2\left(k_x \frac{\tau_a}{4}\right)$$

$$F_1 = \frac{1}{j2k_x\tau_a}\left[\exp\left(jk_x\frac{\tau_a}{2}\right) - \exp\left(jk_x\frac{\tau_a}{4}\right) Sa\left(k_x\frac{\tau_a}{4}\right)\right]$$

and F_1^* is the complex conjugate of F_1.

The set of equations (5) can be represented as

$$\underset{\sim}{Z}\underset{\sim}{I} = 0 \quad (8)$$

where

$$Z = \left[\begin{array}{c|c} Z_{xx\alpha\beta} - R_s F_{x\alpha\beta} & Z_{xy\alpha\beta} \\ \hline Z_{yx\alpha\beta} & Z_{yy\alpha\beta} - R_s F_{y\alpha\beta} \end{array}\right] \quad (9)$$

and

$$I^T = \left[I_{x1}, I_{x2}, \cdots, I_{xP} \,|\, I_{y1}, I_{y2}, \cdots, I_{yQ} \right]. \quad (10)$$

For (8) to have a nontrivial solution, it is necessary that

$$\det Z = 0. \quad (11)$$

This is the dispersion equation which relates k_x to ω. Once k_x has been determined, it is substituted back into the Z matrix so that the eigenvector $\underset{\sim}{I}$ and hence the current density J_s can be found. Numerical examples are discussed in Section VI.

IV. Characteristic Impedance

The presence of apertures and/or resistance precludes the possibility of TEM propagation in the structure of Fig. 1. However, at the frequencies associated with the signal waveforms found in such computer structures ($k_0 d_1 < 0.1$), the wave supported will be nearly TEM. As such, only a small component of magnetic field exists in the direction of propagation, i.e., the line integral of the electric field between the signal line and ground plane in any plane x = constant is nearly independent of path. We can therefore define a potential difference $V(x)$ between the signal line and ground plane as

$$V(x) = -\int_0^h E_z(x, y, z)\, dz \quad (12)$$

where E_z is the z component of the electric field. Since the transmission lines carry signals between computer circuits, and since these circuits are characterized by their current–voltage dependencies, it is convenient to define the characteristic impedance Z_0 as

$$Z_0 = V(x)/I_T(x) \quad (13)$$

where the total current that flows through the signal line I_T is given by

$$I_T = \int_0^{d_2} J_{sx}(z = h)\, dy. \quad (14)$$

In the region which excludes the conductors, the divergence of the electric field is zero so that E_z, E_x, and E_y are related by

$$\frac{\partial E_z}{\partial z} = -\left(\frac{\partial E_x}{\partial x} + \frac{\partial E_y}{\partial y} \right). \quad (15)$$

If we substitute the generalized form of (2) into (15), and integrate both sides of (15) with respect to z, realizing that E_z has no component constant in z, we obtain E_z. The result, after appropriate interchanges in the orders of sum-

mation, integration, and differentiation is

$$E_z = \frac{\eta_0}{2k_0}\left\{ \sum_{\alpha=1}^{P} I_{x\alpha}\,\mathrm{sgn}(z-z_\alpha) \sum_{n,m} G_{xnm\alpha} \cdot \exp(-jk_{znm}|z-z_\alpha|) + \sum_{\alpha=1}^{Q} I_{y\alpha}\,\mathrm{sgn}(z-z_{P+\alpha}) \sum_{n,m} G_{ynm\alpha} \cdot \exp(-jk_{znm}|z-z_{P+\alpha}|) \right\} \exp(-jk_x x) \quad (16)$$

where

$$G_{xnm\alpha} = k_{xn}\mathcal{R}_{xnm}\exp\left\{ j\left[\frac{2\pi n}{d_1}(x_\alpha - x) + \frac{2\pi m}{d_2}(y_\alpha - y) \right] \right\}$$

$$G_{ynm\alpha} = k_{ym}\mathcal{R}_{ynm}\exp\left\{ j\left[\frac{2\pi n}{d_1}(x_{P+\alpha} - x) + \frac{2\pi m}{d_2}(y_{P+\alpha} - y) \right] \right\} \quad (17)$$

and $\mathrm{sgn}(\xi)$ is defined as

$$\mathrm{sgn}(\xi) = \begin{cases} 1, & \xi > 0 \\ -1, & \xi < 0. \end{cases}$$

We now substitute (1) into (14), (16) into (12), and perform the integrations indicated. From (13) we find

$$Z_0 = j\frac{\eta_0}{2k_0}\left[\sum_{\alpha=1}^{P} I_{x\alpha}(\delta_{0,z_\alpha} - \delta_{h,z_\alpha}) \cdot \sum_{n,m} G_{xnm\alpha}\frac{1-\exp(-jk_{znm}h)}{k_{znm}} + \sum_{\alpha=1}^{Q} I_{y\alpha}(\delta_{0,z_{P+\alpha}} - \delta_{h,z_{P+\alpha}}) \cdot \sum_{n,m} G_{ynm\alpha}\frac{1-\exp(-jk_{znm}h)}{k_{znm}} \right] \cdot \left[\tau_b \sum_{\alpha=1}^{P} I_{x\alpha}\delta_{h,z_\alpha} q_{\tau_a}(x-x_\alpha) \right]^{-1}. \quad (18)$$

In (18), $I_{x\alpha}$ and $I_{y\alpha}$ are the current coefficients obtained through solving the eigenvalue problem (8), and q_τ is the triangle function previously defined.

V. Mode Coupling Between Adjacent Signal Lines

It is well known that a system composed of two coupled waveguides supports two distinct propagation modes [9]. A wave traveling along one guide will transfer power to the other guide and may excite positively and negatively propagating waves. Contradirectional coupling [10], involves the transfer of power between modes traveling in opposite directions. With respect to the structure of Fig. 1, this coupling would not significantly differ if the apertures are merged in the x direction, so that the ground plane becomes an array of x-directed strips and the transmission line becomes TEM. Since contradirectional coupling in TEM structures has already been considered [11], we will focus on codirectional coupling [10], which involves the transfer of power between modes traveling in the same direction. This type of coupling is absent in TEM structures.

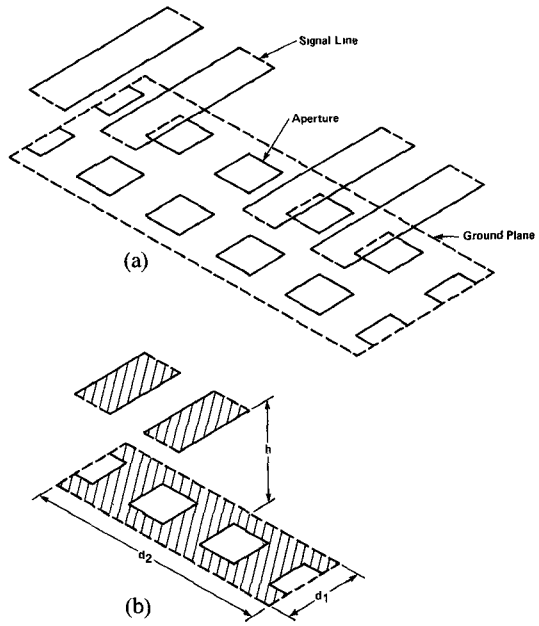

Fig. 3. Guiding structure used in determining the side-by-side coupling. (a) Isometric view. (b) Unit cell.

For two identical waveguides, the power is periodically exchanged between the waveguides and this exchange occurs over a distance l [9] given by

$$\Delta k_x l = \pi \quad (19)$$

where Δk_x is the difference between the coupled system's two propagation constants. In connection with the structure of Fig. 1, these two constants are associated with waves having even and odd symmetry about the plane midway between the lines.

A. Side-by-Side Coupling

If we modify the structure of Fig. 1 by removing every third line, the coupling between nonadjacent lines will be negligible for small h/d_2. Then, the wave in the unit cell will be almost identical to that in a structure having only two adjacent lines. Fig. 3 shows the resulting structure and unit cell.

To get the coupling length l, we find even-mode (where the signal lines carry current in the same direction) and odd-mode (where the lines carry current in opposite directions) solutions to (11), and then substitute the resulting difference in propagation constants Δk_x into (19).

In odd-mode propagation, symmetry allows a perfectly conducting plane to be placed equally distant between the

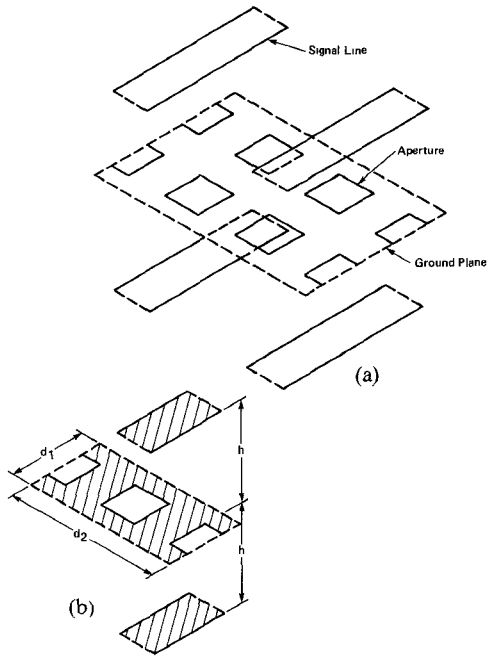

Fig. 4. Guiding structure used in determining the through-aperture coupling. (a) Isometric view. (b) Unit cell.

signal lines without disturbing the field. This plane carries some current that would otherwise flow in the ground plane, decreasing the perturbation caused by the apertures, and causing the wave to be more nearly TEM. Thus, the odd-mode propagation constant will be closer to k_0 than the even-mode constant.

B. Through-Aperture Coupling

We now remove every other line in the structure of Fig. 1, and then place another identical signal-line array a distance h below the ground plane (Fig. 4). As long as h/d_2 is sufficiently small, the wave supported within the unit cell closely resembles that supported by two signal lines situated on opposite sides of the ground plane.

To find l for this through-aperture coupling structure, we again find even- and odd-mode solutions to (11) and substitute the resulting Δk_x into (19). By symmetry, no current flows in the ground plane when the signal lines carry oppositely directed currents. The resulting mode is pure TEM since the ground plane can be removed without disturbing the field. Thus, the odd-mode propagation constant in perfectly conducting structures is k_0, and need not be calculated through (11).

VI. Numerical Results

In solving the eigenvalue problem (8), the solution k_x to the determinant equation (11) is first found by a Newton search [12]. Starting with some initial guess $k_x^{(1)}$, we iterate according to

$$k_x^{(i+1)} = k_x^{(i)} - \frac{\det^i Z}{f^i(Z)} \tag{20}$$

where the superscript i refers to the ith value of the parameter, and $f^i(Z)$ is the finite difference approximation of the determinant's derivative at k_x^i. The iteration is terminated when the difference between $k_x^{(i)}$ and $k_x^{(i+1)}$ is sufficiently small—generally $10^{-5}\ k_0$. When solving (8) for the eigenvector, the first element of $\underline{I}$, I_{x1}, was assumed to have unit amplitude and zero phase. In obtaining the Z matrix (9), we truncate the infinite series in (6) at $|n| \leqslant N$ and $|m| \leq M$ where

$$N = \frac{d_1}{\tau_a}, \quad M = \frac{d_2}{\tau_b}. \tag{21}$$

This choice is adequate to give accurate results. Because the Newton search requires repeated evaluation of the Z matrix, the choice of N and M has a major influence on the overall computation time.

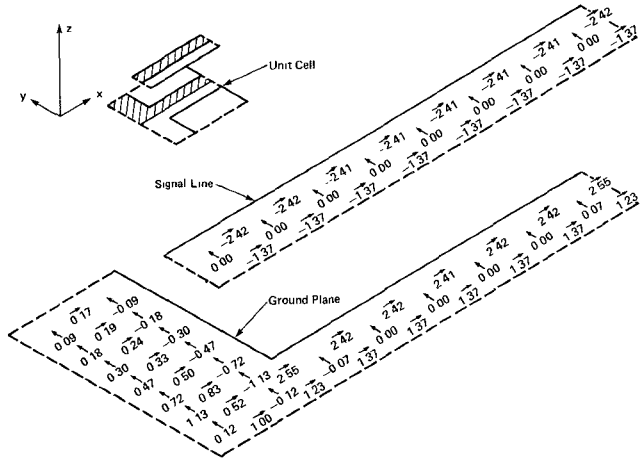

Fig. 5. Current distribution in the signal line and ground plane over half the unit cell of the guiding structure of Fig. 1. ($R_s = 0$, $w = 0.25$ cm, $h = 0.5$ cm, $a = b = 0.75$ cm, $d_1 = d_2 = 1.0$ cm, $k_0 = 0.0001$ cm^{-1}, $N = 8$, $M = 16$.)

A. Current Distribution

Fig. 5 shows the current distribution in the structure of Fig. 1, when $R_s = 0$, $h = 0.5$ cm, $w = 0.25$ cm, $a = b = 0.75$ cm, $d_1 = d_2 = 1.0$ cm, $\tau_a = 0.125$ cm, $\tau_b = 0.0625$ cm, and $k_0 = 0.0001$ cm^{-1}. By symmetry, identical current exists in each half of the unit cell, so only the shaded half is considered.

For this case, the currents are almost entirely real. The x-directed currents in the signal line and ground plane flow in opposite directions. Current crowds along the signal-line edge, displaying the well-known edge effect for perfect conductors, and flows around the aperture in the ground plane. The y-directed current is nearly zero in both the signal line and the ground plane channel defined by the signal-line's projection onto that plane. If we convert the current density into a current by multiplying by τ_b for x-directed currents and by τ_a for y-directed currents, we find the net current which flows into any $\tau_a\tau_b$ patch to be negligible. All these results are consistent with current flow in parallel plate type TEM transmission lines.

Fig. 6 gives the current distribution for the same structure at $k_0 = 0.0001$ cm^{-1}, except the sheet resistance is 0.25 $\Omega/\square$. For such a high sheet resistance and low frequency, the current flow is essentially determined by the resistance, and again is almost entirely real. The x-directed current is

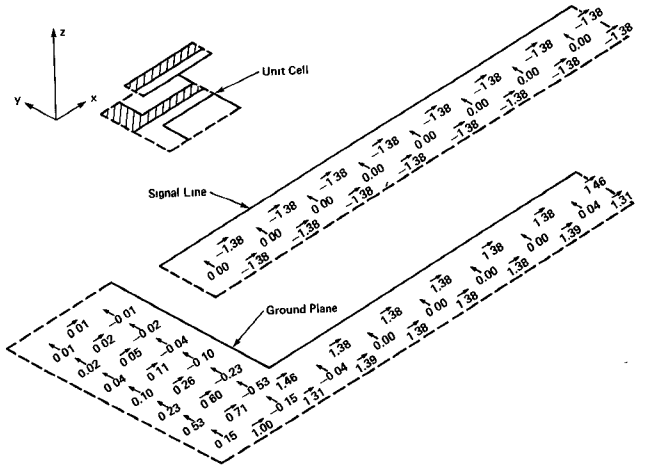

Fig. 6. Current distribution in the signal line and ground plane over half the unit cell of the guiding structure of Fig. 1. ($R_s = 0.25\ \Omega/\square$, $w = 0.25$ cm, $h = 0.5$ cm, $a = b = 0.75$ cm, $d_1 = d_2 = 1.0$ cm, $k_0 = 0.0001$ cm^{-1}, $N = 8$, $M = 16$.)

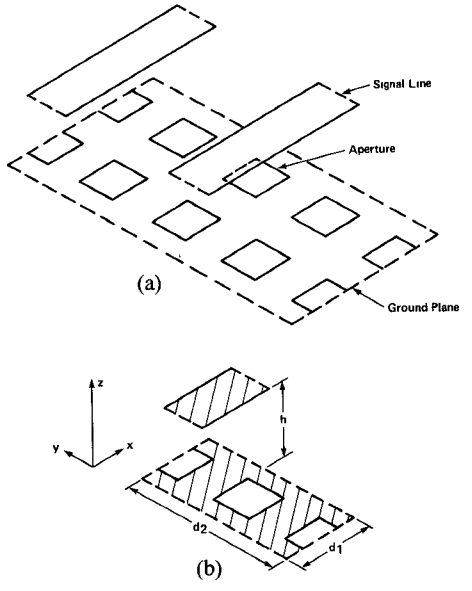

Fig. 7. Guiding structure of Fig. 1 when every other signal line is removed. (a) Isometric view. (b) Unit cell.

uniform across the signal line. The current in the ground plane is more confined to the channel, not spreading out as much into the conductor connecting the channels of adjacent unit cells (called cross-links). For example, the minimum current density in the cross-link is 0.17 when $R_s = 0$, but only 0.01 when $R_s = 0.25\ \Omega/\square$.

B. Propagation Characteristics

To determine the propagation characteristics of an isolated signal line above the ground plane, we consider a modified structure where every other signal line has been removed (Fig. 7(a)). The corresponding unit cell (Fig. 7(b)) contains one signal line but two apertures so that d_2 is doubled.

Fig. 8 shows the dispersion curve when w, h, a, b, τ_a, τ_b, and d_1 are as previously given, but $R_s = 0$ and $d_2 = 2.0$ cm.

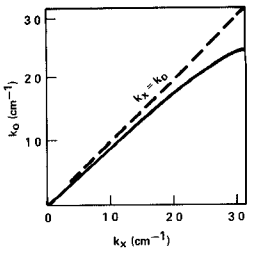

Fig. 8. Wave number versus propagation constant for the guiding structure of Fig. 7. ($R_s = 0$, $w = 0.25$ cm, $h = 0.5$ cm, $a = b = 0.75$ cm, $d_1 = 1.0$ cm, $d_2 = 2.0$ cm, $\tau_a = 0.125$ cm, $\tau_b = 0.0625$ cm, $N = 8$, $M = 32$.)

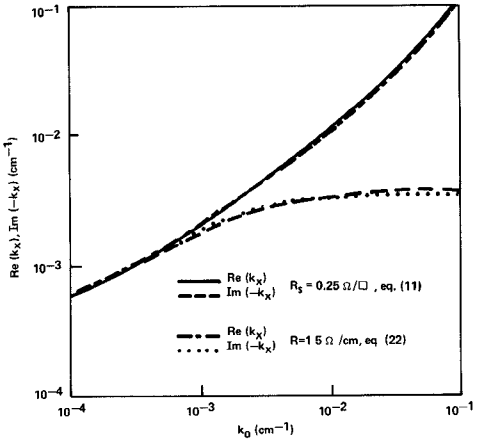

Fig. 9. Real and imaginary parts of k_x as a function of k_0 for the guiding structure of Fig. 7. ($w = 0.25$ cm, $h = 0.5$ cm, $a = b = 0.75$ cm, $d_1 = 1.0$ cm, $d_2 = 2.0$ cm, $\tau_a = 0.125$ cm, $\tau_b = 0.0625$ cm, $N = 8$, $M = 32$.)

The ratio of group velocity v_g to the speed of light in the dielectric c is given by the curve's slope. For small k_x, v_g/c is a constant 0.9606, but decreases to zero for $k_x d_1 = \pi$, as expected for periodic structures.

Fig. 9 gives the real and imaginary parts of k_x as a function of k_0 when R_s is 0.25 $\Omega/\square$. For comparison, we also plot the propagation constant calculated from the well-known formula valid for a resistive transmission line having lossless dielectric

$$k_x = [(\omega L - jR)\omega C]^{1/2}. \tag{22}$$

In (22), L and C, which are per unit length values of capacitance and inductance, are taken to be those values which give the same low-frequency propagation constant ($k_x = 1.0352\ k_0$) and characteristic impedance (216 Ω) found for the case $R_s = 0$; R, the per unit length resistance, is taken to be the dc resistance in the path that includes the signal line and ground plane. The values for L and C are 7.44 nh/cm and 0.16 pf/cm, respectively, while R is approximated as 1.5 Ω/cm. As seen from the figure, (22) accurately gives the low frequency propagation constant for resistive conductors.

The characteristic impedance, calculated at the center of the signal line using (18), is plotted versus k_0 in Fig. 10 for $R_s = 0$ and 0.25 $\Omega/\square$. For comparison, we also plot the equation

$$Z_0 = [(R + j\omega L)/j\omega C]^{1/2} \tag{23}$$

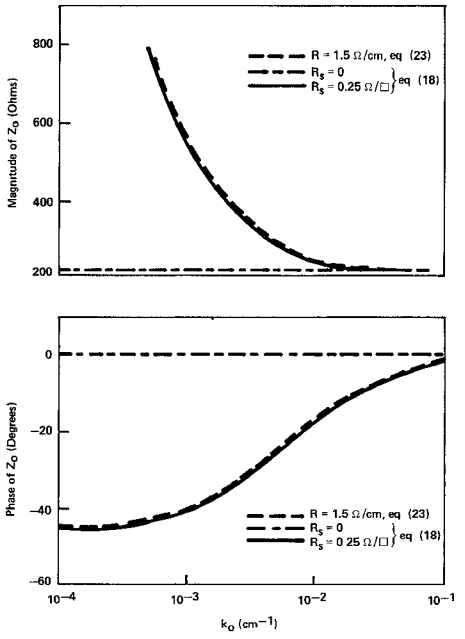

Fig. 10. Characteristic impedance versus k_0 for the guiding structure of Fig. 7. ($w = 0.25$ cm, $h = 0.5$ cm, $a = b = 0.75$ cm, $d_1 = 1.0$ cm, $d_2 = 2.0$ cm, $\tau_a = 0.125$ cm, $\tau_b = 0.0625$ cm, $N = 8$, $M = 32$.)

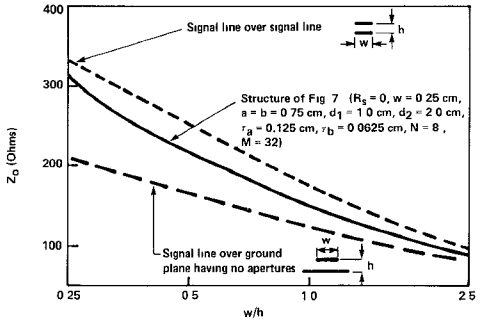

Fig. 11. Characteristic impedance as a function of signal line width-to-height ratio w/h ($R_s = 0$, $k_0 = 0.001$ cm^{-1}).

where R, L, and C have already been calculated. As seen from Fig. 10, (23) accurately describes the impedance for $k_0 d_1 < 0.1$.

The dependence of the impedance at low frequency on the aspect ratio w/h is shown in Fig. 11. The curves are obtained by holding w fixed at 0.25 cm and varying h. For comparison, the impedance of an isolated signal line above a ground plane having no apertures, and that of an isolated signal line a height h above a second such line have been plotted. The impedance for this first nonperiodic structure is given in [13], while the impedance for the second is obtained from [13] using image theory. As expected, the impedance of the periodic structure falls between the other two curves. However, as w/h falls below 0.25, the coupling between adjacent signal lines significantly influences Z_0, and the curve displays a sharp up-turn.

The influence of adjacent lines can also be observed by replacing the lines absent from the structure of Fig. 7. Although the resulting dispersion and impedance curves display similar behavior to those in Fig. 8 and Fig. 9, the group velocity and impedance when $R_s = 0$ and $k_0 d_1 \ll 1$ are 0.9505 c and 290 Ω, respectively, as opposed to 0.9606 c and 216 Ω for the structure of Fig. 7.

TABLE I
NORMALIZED COUPLING LENGTH AT $k_0 = 0.001$ cm^{-1}

Coupling	Unit Cell	k_x/k_0 (Even Mode)	k_x/k_0 (Odd Mode)	$\Delta k_x/k_0$	l/λ_0
Side-By-Side	(a)	1 0420	1 0039	0 0381	13 12
Through-Aperture	(b)	1 0653	1 0000	0 0653	7 66

$R_s = 0$, $w = 0.25$ cm, $h = 0.5$ cm, $a = b = 0.75$ cm, $d_1 = 1.0$ cm, $\tau_a = 0.125$ cm, $\tau_b = 0.0625$ cm, $N = 8$.
(a) Unit cell of Fig. 3. ($d_2 = 3.0$ cm, $M = 48$).
(b) Unit cell of Fig. 4. ($d_2 = 2.0$ cm, $M = 32$).

In order to determine the sensitivity of the results to the size of the subsections, τ_a and τ_b were reduced by a factor of two (increasing the corresponding number of current elements, $P + Q$, by more than a factor of four). For the structure considered in Fig. 5, with h varied between 0.1 and 1.0 cm, and with N and M still given by (21), we observed that both k_x and Z_0 decrease, but by less than 0.3 percent and 4.0 percent, respectively. Thus, the subsection size used for the structures considered is adequate to give accurate results.

It is instructive to determine the changes in capacitance and inductance when the perforated ground plane becomes unperforated. To do this, we modify the structure considered in Fig. 8 so that $a = 0.0$ cm and use $R_s = 0$, $\tau_a = 1.0$ cm, $N = 0$, and $M = 32$. The values of L and C are then calculated from the resulting values of k_x and Z_0. We find at low frequency that the capacitance increases by 6.3 percent but the inductance decreases by 12.2 percent. Thus, the perforated ground plane acts more like an unperforated plane electrostatically than it does magnetostatically.

C. Coupling Between Adjacent Signal Lines

The side-by-side and through-aperture coupling lengths are calculated using the structures of Fig. 3 and Fig. 4 for $R_s = 0$, $h = 0.5$ cm, $w = 0.25$ cm, $a = b = 0.75$ cm, $d_1 = 1.0$ cm, $\tau_a = 0.125$ cm, $\tau_b = 0.0625$ cm, and $k_0 = 0.001$ cm^{-1}. The even- and odd-mode propagation constants, shown normalized in Table I, increase slowly with k_0 so that they are valid for $k_0 d_1 < 0.1$. The normalized coupling length for the side-by-side case is 13.12 λ_0, but only 7.66 λ_0 for the through-aperture case. The greater through-aperture coupling (smaller l/λ_0) corresponds to a greater difference between capacitive and inductive coupling coefficients, k_C and k_L, that exist in the structure [11]. Though not true for all geometries, the cross-link segments of the ground plane substantially reduce the capacitive coupling between signal lines separated by the ground plane, but only modestly decrease the inductive coupling and thus yield the shorter value of l.

VII. Extension of the Method Through Scaling

In the examples given, all the dimensions were in the centimeter range, while the relative dielectric constant was unity. However, in computer applications, the transmission line dimensions may be in the submillimeter range, and the

dielectric constant may be several times that of free space. Appropriate scaling can be used to extend the presented results to more realistic structures.

If every dimension in the structure scales by the same factor, and if the relative dielectric constant takes on the value ϵ_r, the dispersion relation represented by (5) can be expressed as

$$f_1\left(k_0\sqrt{\epsilon_r}d_1, k_x d_1\right)+\sqrt{\epsilon_r}R_s f_2(k_x d_1)=0$$

while the characteristic impedance can be expressed as

$$Z_0=\frac{1}{\sqrt{\epsilon_r}}f_3\left(k_0\sqrt{\epsilon_r}d_1, k_x d_1\right)$$

where f_1, f_2, and f_3 are functions of the given variables. Thus, the dispersion relation will remain satisfied and the impedance will vary inversely with $\sqrt{\epsilon_r}$ if $k_x d_1$, $k_0\sqrt{\epsilon_r}d_1$, and $\sqrt{\epsilon_r}R_s$ are kept constant.

VIII. Conclusions

A method employing a rooftop current approximation was used to find the propagation characteristics and current distribution in transmission-line structures consisting of a signal line above a periodically perforated ground plane in a homogeneous dielectric. For perfect conductors at low frequency ($k_0 d_1 < 1.0$), the dispersion is small and the wave velocity is just a few percent less than c. For finite resistance structures at frequencies such that $k_0 d_1 < 0.1$, the propagation and attenuation constants, and the impedance, are the same as those of a uniform transmission line having constant values of R, L, and C.

Codirectional coupling between signal lines was considered. This coupling was found to be nearly twice as strong for signal lines situated on opposite sides of the ground plane (coupling length 7.66 λ_0) as for adjacent signal lines situated on the same side of the ground plane (coupling length 13.12 λ_0). These results, however, are valid only for frequencies such that $k_0 d_1 < 0.1$ and for the specific geometry considered.

Although we have considered only square apertures, the method applies to any shape aperture for which the conductor can be subdivided into rectangular subsections. Apertures with curved boundaries, such as circles, would have to be approximated by steps. Finally, the approach used here can easily be extended to handle additional ground planes.

References

[1] A. J. Blodgett and D. R. Barbour, "Thermal conduction module: A high performance multilayer ceramic package," *IBM J. Res. Develop.*, vol. 26, no. 1, pp. 30–36, Jan. 1982.

[2] A. E. Ruehli and P. A. Brennan, "Efficient capacitance calculations for three dimensional multiconductor systems," *IEEE Trans. Microwave Theory Tech.*, vol. MTT-21, pp. 76–82, Feb. 1973.

[3] A. E. Ruehli, "Inductance calculations in a complex integrated circuit environment," *IBM J. Res. Develop.*, vol. 16, no. 5, pp. 470–481, Sept. 1972.

[4] R. E. Collin, *Field Theory of Guided Waves*. New York: McGraw-Hill, 1960, ch. 9, pp. 368–371.

[5] Born and Wolf, *Principles of Optics*. Oxford: Pergamon Press, 1959, ch. 11.5.

[6] A. W. Glisson and D. R. Wilton, "Simple and efficient numerical methods for problems of electromagnetic radiation and scattering from surfaces," *IEEE Trans. Antennas Propagat.*, vol. AP-25, pp. 593–607, Sept. 1980.

[7] B. J. Rubin and H. L. Bertoni, "Reflection from a periodically perforated plane using a subsectional current approximation," *IEEE Trans. Antennas Propagat.*, (accepted for publication).

[8] B. J. Rubin, "Scattering and guiding of electromagnetic waves by screens with periodic apertures," Ph.D. dissertation, Polytechnic Institute of New York, New York, NY, 1982.

[9] D. A. Watkins, *Topics in Electromagnetic Theory*. New York: Wiley, 1958.

[10] C. C. Johnson, *Field and Wave Electrodynamics*. New York: McGraw-Hill, 1965.

[11] M. K. Krage and G. I. Haddad, "Characteristics of coupled microstrip transmission lines—I: Coupled-mode formulation of inhomogeneous lines," *IEEE Trans. Microwave Theory Tech.*, vol. MTT-18, pp. 217–222, Apr. 1970.

[12] S. D. Conte and C. de Boor, *Elementary Numerical Analysis*, 2nd ed. New York: McGraw-Hill, 1965.

[13] H. A. Wheeler, "Transmission-line properties of parallel strips separated by a dielectric sheet," *IEEE Trans. Microwave Theory Tech.*, vol. MTT-13, pp. 172–185, Mar. 1965.

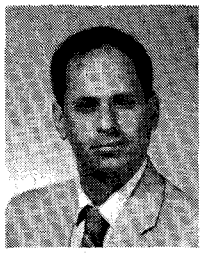

Barry J. Rubin was born in New York City in 1952. He received the B.E.E.E. degree from the City College of New York in 1974.

He joined the International Business Machines Corporation in 1974 and received the M.S.E.E. degree from Syracuse University, New York, in 1978, and received the Ph.D degree from the Polytechnic Institute of New York in 1982. He has worked on power transistor design, CCD technology, circuit design, and since 1976, on electrical packaging analysis. He has been awarded five U.S. patents.

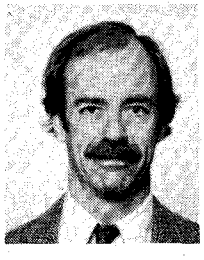

Henry L. Bertoni (M'67–SM'80) was born in Chicago, IL, on November 15, 1938. He received the B.S. degree in electrical engineering from Northwestern University, Evanston, IL, in 1960, the M.S. degree in electrical engineering in 1962, and the Ph.D. degree in electrophysics in 1967, both from the Polytechnic Institute of Brooklyn (now of New York), Brooklyn, NY.

In 1966 he joined the faculty of the Polytechnic Institute of New York, and now holds the rank of Professor in the Department of Electrical Engineering and Computer Science. He was elected Speaker of the Faculty for 1981–1982. Since 1967 he has served as a consultant in the areas of radar, ultrasonics, and radio propagation. His research has dealt with various aspects of wave propagation and scattering. These include the geometrical theory of diffraction, electromagnetic and optical waves in multilayered and periodic structures, magnetoelastic waves, and ultrasonics as applied to both signal processing and nondestructive evaluation. He is a member of the Acoustical Society of America, the International Scientific Radio Union, and Sigma Xi.